BMC Cancer

RESEARCH Open Access

Prediction of disease-free survival using strain elastography and diffuse optical tomography in patients with T1 breast cancer: a 10-year follow-up study

Jing Zhang[1†], Hao Sun[2†], Song Gao[3], Ye Kang[4] and Cong Shang[1*]

Abstract

Background Early-stage breast cancer (BC) presents a certain risk of recurrence, leading to variable prognoses and complicating individualized management. Yet, preoperative noninvasive tools for accurate prediction of disease-free survival (DFS) are lacking. This study assessed the potential of strain elastography (SE) and diffuse optical tomography (DOT) for non-invasive preoperative prediction of recurrence in T1 BC and developed a prediction model for estimating the probability of DFS.

Methods A total of 565 eligible patients with T1 invasive BC were enrolled prospectively and followed to investigate the recurrence. The associations between imaging features and DFS were evaluated and a best-prediction model for DFS was developed and validated.

Results During the median follow-up period of 10.8 years, 77 patients (13.6%) developed recurrences. The fully adjusted Cox proportional hazards model showed a significant trend between an increasing strain ratio (SR) ($P < 0.001$ for trend) and the total hemoglobin concentration (TTHC) ($P = 0.001$ for trend) and DFS. In the subgroup analysis, an intensified association between SR and DFS was observed among women who were progesterone receptor (PR)-positive, lower Ki-67 expression, HER2 negative, and without adjuvant chemotherapy and without Herceptin treatment (all $P < 0.05$ for interaction). Significant interactions between TTHC status and the lymphovascular invasion, estrogen receptor (ER) status, PR status, HER2 status, and Herceptin treatment were found for DFS($P < 0.05$).The imaging–clinical combined model (TTHC + SR + clinicopathological variables) proved to be the best prediction model (AUC = 0.829, 95% CI = 0.786–0.872) and was identified as a potential risk stratification tool to discriminate the risk probability of recurrence.

Conclusion The combined imaging-clinical model we developed outperformed traditional clinical prognostic indicators, providing a non-invasive, reliable tool for preoperative DFS risk stratification and personalized therapeutic

†Jing Zhang and Hao Sun contributed equally to this work.

*Correspondence:
Cong Shang
shangc@cmu.edu.cn

Full list of author information is available at the end of the article

strategies in T1 BC. These findings underscore the importance of integrating advanced imaging techniques into clinical practice and offer support for future research to validate and expand on these predictive methodologies.

Keywords Breast cancer, Prognosis, Recurrence, Prediction, Optical, Strain elastography

Background

Improvements in screening strategies and public awareness have increased the prevalence of patients presenting with T1 breast cancer (BC), which have tumors ≤ 2 cm in size [1]. Generally, these small tumors have relatively good prognoses, and most of them do not require systemic adjuvant treatment [2]. However, they comprise a heterogeneous group, and many studies have identified biologically defined at-risk patients with T1 BC [2, 3]. Long-term follow-up studies have shown that the recurrence rate, which is an independent prognostic factor contributing to mortality, was up to 20% of cases at 10–20 years [4]. Thus, identifying predictive factors and estimating the risk of recurrence are important for managing patients with T1 BC. The increased selection of neoadjuvant treatment has made the preoperative prediction of clinical outcomes ever more important despite the small tumor size. This aids in understanding the natural course of the disease and in deciding the proper treatment.

Traditionally, surgical specimens are required to obtain most classical prognostic factors, including tumor size, clinical TNM stage, grade, lymph node status, Ki-67, and estrogen receptor (ER) / progesterone receptor (PR) status [5, 6]. Most histopathological data are available preoperatively from breast core-needle biopsy; however, this diagnostic method is invasive, and the predictive power of clinical indicators alone is controversial. Multigene assays can provide prognostic information related to the risk of recurrence; however, genetic testing is costly, and its clinical utility has been established only in certain subsets of patients [7–9].

Studies focused on the application of imaging modalities for the preoperative assessment of prognoses have evaluated several predictive indicators [10–13]. Although MRI and PET have certain predictive values for prognoses, there are constraints to their practical application: cost, the use of contrast agents, and ionizing radiation from PET. Ultrasound (US) is the preferred first-line imaging modality for BC; however, conventional US does not predict prognoses well [14]. Non-invasive pre-operative tools that accurately predict individual clinical outcomes of T1 BC are currently lacking, and new imaging indicators are urgently needed.

Ultrasound elastography (UE) is a non-invasive imaging technique that can visualize and quantify tissue stiffness, which is an important factor in the tumor microenvironment. Elastography strain in BC lesions is significantly associated with prognostic factors [15, 16], suggesting that the strain ratio (SR) may be associated with BC prognosis. However, few studies have investigated the predictive ability of the SR for prognosis in BC, especially T1 BC.

Ultrasound-guided diffuse optical tomography (US-guided DOT) uses non-invasive near-infrared light to measure the optical absorption and scattering properties of tissues. The primary output data is the total hemoglobin concentration (TTHC), which indirectly reflects the tumor's blood supply. Tumor angiogenesis, another key component of the tumor microenvironment, is a rate-limiting step of tumor growth and progression and may have prognostic significance [17, 18]; nevertheless, few studies have addressed this relationship [18, 19].

Tumor stiffness and blood flow characteristics are associated with the prognosis of BC. To our knowledge, these findings have not been comprehensively evaluated in T1 BC. This 10-year follow-up study explored the relationship of disease-free survival (DFS) with the pre-surgical SR and TTHC in patients with T1 BC to predict recurrence among the whole population or a predefined subgroup. BC-related clinicopathological prognostic parameters were combined to develop a novel DFS prediction model to improve preoperative risk stratification for customized management of T1 BC patients.

Patients and methods

Study population

Between January 2012 and December 2014, 1255 consecutive women who were candidates for surgical resection of US-suspected breast lesions were enrolled. The inclusion criteria were as follows: US-suspected breast masses; women aged 18–80 years; maximum diameter of lesions on US ≤ 2.00 cm; surgery as initial treatment without neoadjuvant chemotherapy, radiation, or other therapies; complete preoperative imaging evaluation (UE and DOT); pathological diagnosis of invasive BC; and available postsurgical immunohistochemical data. Patients were excluded if they had benign breast lesions or carcinoma in situ, distant metastases, a history of BC or any other malignancy, severe comorbidities, multifocal lesions or bilateral disease, or unavailable image data. Finally, the study included 565 breast tumors (mean size: 1.46 ± 0.389 cm, range: 0.2–2.0 cm) in 565 women (mean age: 50.95 years, range: 27–78 years). A flowchart of the study's selection process is shown in Fig. 1.

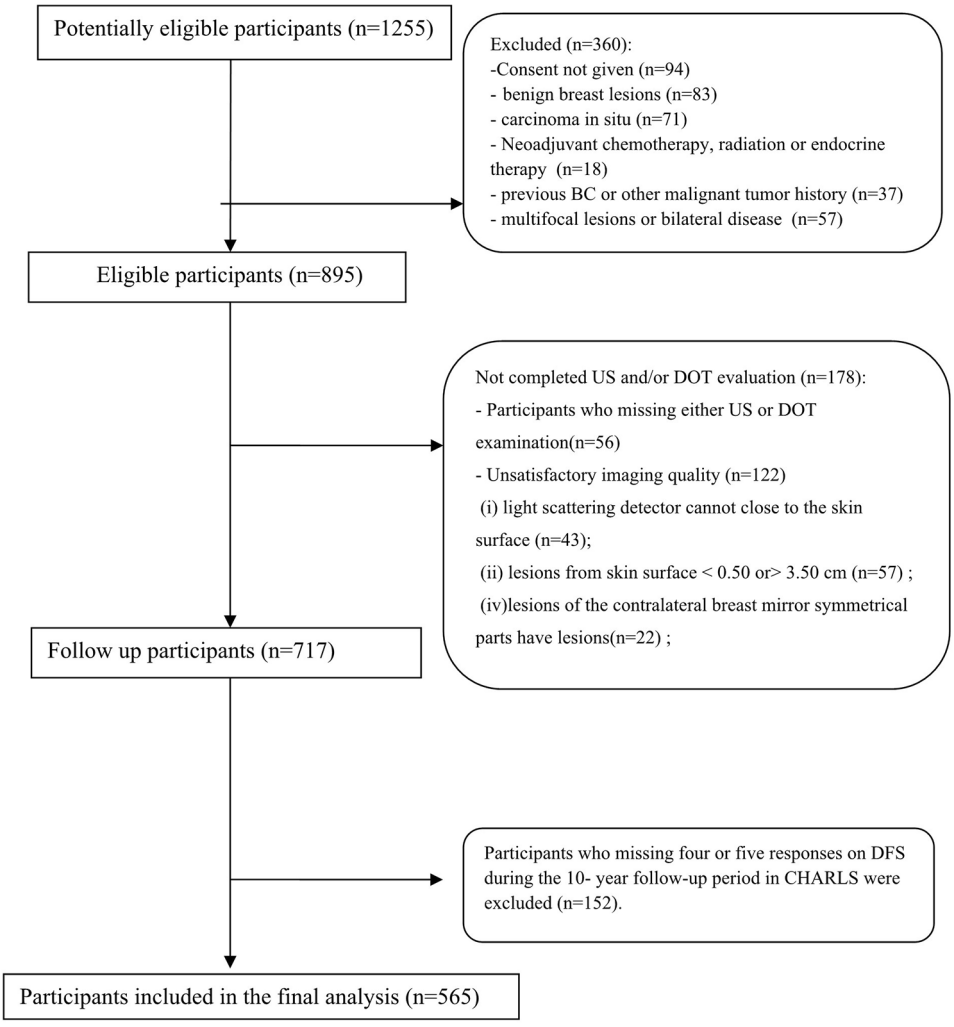

Fig. 1 Flow chart of the study's selection process

Preoperative imaging evaluation (strain elastography and US-guided DOT)

The day prior to surgery, double-blind strain elastography (SE) and US-guided DOT evaluations were independently conducted by two board-certified radiologists, each with over 5 years of experience in breast imaging and more than 500 image evaluations of breast SE and US-guided DOT, meeting the professional standard of proficiency [20, 21]. They were blinded to clinicopathological features and clinical data. The SE and DOT examinations and data analyses commenced with a training phase involving the examination of images from at least 20 cases. This training phase was supervised by two professional technicians following manufacturers' standard operating procedures.

Gray-scale and elastography images were obtained using an HV-900 US system (Hitachi Medical Corporation, Tokyo, Japan) with a 6–13 MHz linear transducer. The BI-RADS category of each mass was determined according to the ACR guidelines [22]. During SE, the patients were instructed to relax and breathe normally. Four SE images from the maximal-diameter plane of the lesion and its orthogonal plane were obtained for each lesion. The elastography sampling frame was set to include the targeted lesion and surrounding normal tissue, with the depth ranging from the subcutaneous fat to the pectoral muscle and the width covering the entire examination range. The elastogram images were generated by applying appropriate compression to the skin above the targeted breast lesion; pressure indicator values ranging from 3 to 4 were considered optimal. Region of interest (ROI) A was drawn manually to include the lesion; ROI B was selected to include subcutaneous fat tissue and exclude the lesion, without specific constraints for ROI shape and area [23]. Finally, the SR, which is defined as the fat-to-mass strain ratio, was calculated automatically. The SR measurements from the four images were averaged, and the average value was used for analysis.

On the same day after the UE examination, US-guided DOT was performed using an OPTIMUS Type II breast diagnostic system (XinaoMDT Technology Co., Ltd., China). This system is equipped with a diagnostic US device (Terason T3000 US system with a linear 7–12 MHz probe; Teratech, USA) and a DOT system. Tumors were first located using conventional US, and optical imaging was then performed using a handheld probe. The optical fiber emits near-infrared light (785 and 830 nm) to scan the tumor tissue and the corresponding normal area in the contralateral breast. The tissue absorption and scattering data at different depths can be compared to the corresponding sites of the bilateral breast tissue for evaluation. Finally, the tissue TTHC optical parameter was obtained by defining the ROI manually.

On the DOT map, different colors are used to indicate different absorption intensities. Red indicates increased photon absorption and a greater TTHC; blue indicates decreased photon absorption and a lower TTHC. The data were measured four times and averaged.

As described above, Inter-observer variability was evaluated by having a second radiologist, blinded to the initial results, repeat the measurements. Both radiologists possessed equal levels of experience.

Histopathological analysis

All patients underwent primary tumor resection via mastectomy or breast-conserving surgery; all resected specimens were confirmed histopathologically by the Pathology Department. Histological diagnosis of each tissue specimen was examined by two pathologists independently in a blinded manner, each possessing 10 years of experience in histological breast evaluation. Any discrepancies in histological diagnosis were resolved through discussion between the two pathologists until consensus was reached. The tumor histological characteristics and immunohistochemical factors were recorded. Positive staining for ER/PR was defined as nuclear staining in ≥1% of tumor cells [24]. HER2 positivity was defined as membrane staining of 3+or HER2 gene amplification [25]. The number of Ki-67-positive nuclei per 1000 tumor cell nuclei was recorded as the Ki-67 index. The cutoff point for Ki-67 positivity was 14% [26]. Tumors were classified into four molecular subtypes: Luminal A, Luminal B, HER2+, and triple negative [26]. All other histopathological data were evaluated based on well-accepted international criteria [27, 28].

Postoperative care and follow-up

Postoperative adjuvant treatments, including chemotherapy, radiotherapy, and endocrine therapy, were administered depending on the tumor characteristics and clinical practice. From the first day after surgery, patients were followed-up every 6 months for the first two years and annually thereafter. The primary endpoint was DFS, which was defined as the time from the date of surgery to the first invasive recurrence or the last follow-up visit, whichever came first. Recurrence refers to locoregional recurrence, distant metastasis, or new primary invasive contralateral BC [29]. Follow-up information was collected using outpatient reviews or telephone follow-ups. The final follow-up date was December 31, 2023.

Statistical analysis

All analyses were performed using R software (version 4.2.1; R Foundation for Statistical Computing, Vienna, Austria), and two-tailed P-values <0.05 were considered statistically significant. Continuous variables with normal distribution are expressed as the mean ± standard deviation (SD); categorical variables are described as numbers (percentages). The intraclass correlation coefficient (ICC) was calculated to assess the inter-observer reproducibility for the SR and TTHC measurements.

Log-rank method analysis was performed to explore the relationship between clinicopathological and imaging variables and recurrence outcomes; variables with $P<0.10$ were considered potential associated factors. The relationships between SR, TTHC, and DFS were analyzed with Cox proportional hazards regression using three different adjustment models: unadjusted (model 1), adjusted for age and menopausal status (model 2), and model 2 plus potential associated factors (model 3). The continuous SR and TTHC data were converted into categorical variables according to the tertiles of TTHC and SR. The trend across all categorical variables was tested by coding each tertile variable with the median SR or TTHC value and using it as a continuous variable in Cox proportional hazards regression.

Subgroup analysis was performed to explore whether the associations between SR or TTHC and DFS differed among different groups of patients. Subgroup analysis was performed using Cox proportional hazards regression, including variables for the SR or TTHC level (categorical), subgroup, possible confounding factors, and an interaction term (SR/TTHC × subgroup), which represents subgroup differences in different SR or TTHC categories. Differences were considered statistically significant if the interaction had a P-value <0.05.

Four different models were developed using Cox proportional hazards regression: a classical clinical model (C), TTHC+C, SR+C, and TTHC+SR+C. For each model, the area under the ROC curve (AUC), sensitivity, specificity, accuracy, negative predictive value, and positive predictive value were calculated to compare the model prediction performance, and a nomogram summarizing the best model was established.

For the best prediction model, decision curve analysis was performed to assess the potential clinical usefulness and clinical net benefit at different threshold probabilities. To examine the prediction model's ability to stratify the risk of recurrence, BC patients were divided into three groups (low, medium, and high risk) by tertiles based on estimated risk and compared across tertiles.

Results

Baseline characteristics of the patients

Supplemental Table 1 presents the baseline demographic and clinicopathological characteristics of the 565 patients with T1 BC (tumor size≤2 cm), including 99 patients with a tumor size≤1 cm. Among the patients, 507 underwent a mastectomy and 58 underwent conserving surgery. The histological features of the primary tumors included invasive ductal carcinoma in 534 patients (94.5%) and invasive lobular carcinoma in 31 patients (5.5%). Among the molecular subtypes, Luminal A, Luminal B, HER2+, and triple-negative subtypes accounted for 34%, 24.6%, 26.7%, and 14.7% of the total cases, respectively. Additionally, 481 patients (85.1%) were diagnosed with stage I or II disease and 84 (14.9%) had advanced stage III disease. With a median follow-up time of 130 months (range: 7–156 months), 77 patients developed recurrence with a median DFS time of 41 months. The recurrences in the confirmed cases were located in the bone (27), lungs (21), brain (8), axillary and supraclavicular lymph nodes (5), and multiple organs (16). The means of the SRs and TTHCs were 4.50 and 197.67 μmol/L, respectively, with excellent inter-observer reliability (ICC=0.88 and ICC=0.86, respectively). Figure 2 shows the findings of the preoperative imaging and subsequent PET-CT follow-up of one case of recurrence.

Relationship between clinicopathological and imaging features and DFS in univariate analysis

Univariate Cox regression analysis of clinicopathological and imaging features for DFS is shown in Table 1. For clinicopathological factors, DFS was associated with molecular subtype, initial clinical stage, histological grade, lymphovascular invasion, Ki-67 status, radiation, and adjuvant chemotherapy, with crude hazard ratios (HRs) of 2.22, 3.27, 2.26, 2.91, 2.52, 2.03, and 2.03,

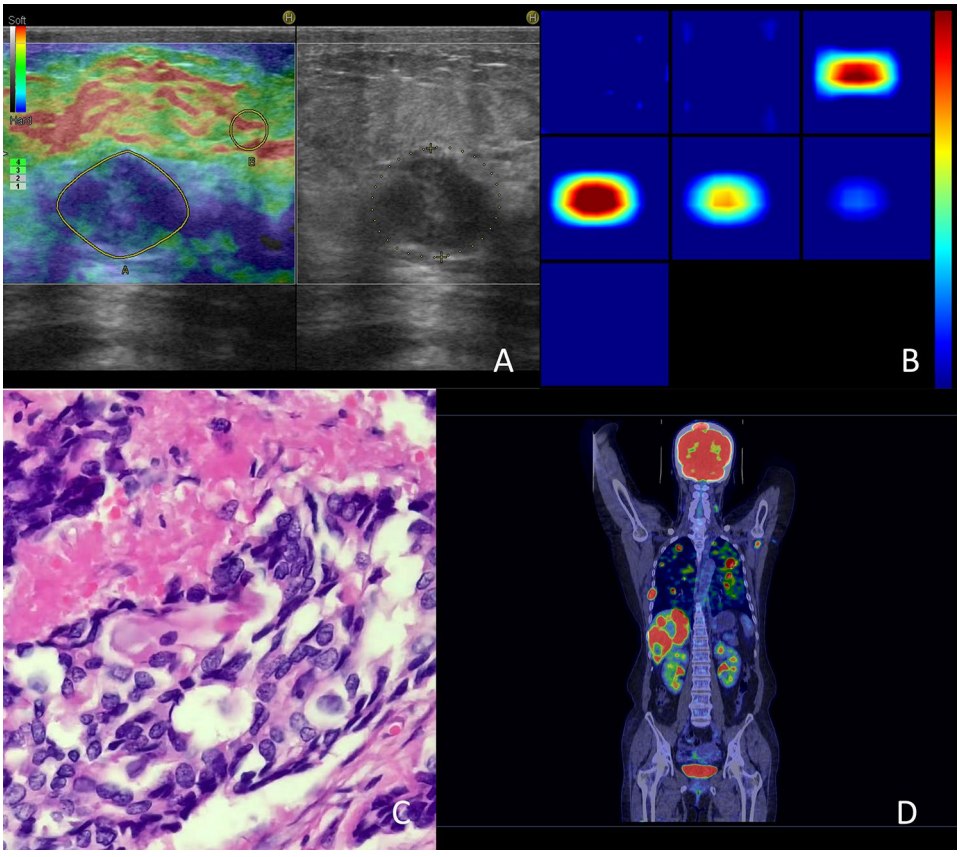

Fig. 2 Findings on preoperative imaging and PET-CT follow-ups of one recurrence case. A 48-year-old woman presented with invasive ductal carcinoma with multiple new long-term metastases. (**A**) On the ultrasound elastography image (left), the strain ratio of the breast tumor is 8.35. (**B**) Diffuse optical tomography of the tumor shows remarkable absorption. The TTHC is 281.253 μmol/L. (**C**) A surgical histopathological section reveals that the tumor is an invasive ductal breast carcinoma (H&E stain, original magnification ×100, scale bar: 100 μm). (**D**) A whole-body 18 F-fluciclovine PET-CT scan reveals multiple metastases in the axillary lymph nodes, liver, lungs, parietal bone, and ribs 112 months (9 years) after surgery

Table 1 Univariate Cox regression analysis for DFS predicted by clinicopathological and imaging characteristics

	No recurrence (*n* =488)	Recurrence (*n* =77)	Hazard ratio	95% CI	*P* value
Age (y)					
<45	118(24.2)	16(20.8)	1(Reference)		
>=45	370(75.8)	61(79.2)	1.19	0.69-2.07	0.53
Menopausal status					
Premenopausal	290(59.4)	42(54.5)	1		
Postmenopausal	198(40.6)	35(45.5)	1.2	0.76-1.87	0.43
Molecular subtype					
Luminal A	174(35.7)	18(23.4)	1		
Luminal B	112(23.0)	27(35.1)	2.22	1.22-4.04	**0.009**
HER2 positive	131(26.8)	20(26.0)	1.47	0.78-2.78	0.24
Triple negative	71(14.5)	12(15.6)	1.67	0.81-3.47	0.17
Pathological types					
Invasive ductal carcinoma	460(94.3)	74(96.1)	1		
Invasive lobular carcinoma	28(5.7)	3(3.9)	0.68	0.21-2.15	0.51
Tumor size					
<=1 cm	90(18.4)	9(11.7)	1		
<=2 cm	398(81.6)	68(88.3)	1.62	0.81-3.25	0.17
Initial clinical stage					
I/II	431(88.3)	50(64.9)	1		
III	57(11.7)	27(35.1)	3.27	2.05-5.22	**<0.001**
Histological grade					
I /II	433(88.7)	59(76.6)	1		
III	55(11.3)	18(23.4)	2.26	1.34-3.84	**0.002**
Nodal status					
NO	280(57.4)	37(48.1)	1		
YES	208(42.6)	40(51.9)	1.38	0.88-2.15	0.16
Lymphovascular invasion					
Negative	440(90.2)	57(74.0)	1		
Positive	48(9.8)	20(26.0)	2.91	1.75-4.85	**<0.001**
ER					
Negative	143(29.3)	28(36.4)	1		
Positive	345(70.7)	49(63.6)	0.71	0.45-1.13	0.71
PR					
Negative	146(29.9)	26(33.8)	1		
Positive	342(70.1)	51(66.2)	0.82	0.51-1.32	0.42
HER2					
Negative	356(73.0)	57(74.0)	1		
Positive	132(27.0)	20(26.0)	0.95	0.57-1.59	0.86
Ki-67					
<=14%	266(54.5)	24(31.2)	1		
>14%	222(45.5)	53(68.8)	2.52	1.55-4.07	**<0.001**
Type of surgery					
Breast-conserving	54(11.1)	4(5.2)	1		
Total mastectomy	434(88.9)	73(94.8)	2.15	0.79-5.88	0.14
Radiation					
No	376(77.0)	46(59.7)	1		
Yes	112(23.0)	31(40.3)	2.03	1.29-3.20	**0.002**
Adjuvant chemotherapy					
No	245(50.2)	25(32.5)	1		
Yes	243(49.8)	52(67.5)	2.03	1.26-3.28	**0.004**
Adjuvant hormone therapy					
No	128(26.2)	26(33.8)	1		

Table 1 (continued)

	No recurrence	Recurrence	Hazard ratio	95% CI	*P* value
	(*n* =488)	(*n* =77)			
Yes	360(73.8)	51 (66.2)	0.68	0.43-1.09	0.11
Herceptin treatment					
No	353(72.3)	57(74.0)	1		
Yes	135(27.7)	20(26.0)	0.93	0.56-1.54	0.77
Imaging variable					
BI-RADS					
3/4a	14(2.9)	2(2.6)	1		
4b	107(21.9)	9(11.7)	0.65	0.14-3.03	0.59
4c	144(29.5)	21(27.3)	1.1	0.26-4.69	0.9
5	223(45.7)	45(58.4)	1.46	0.36-6.03	0.6
SR (mean ±SD)	4.30±1.93	5.81±2.26	1.28	1.17-1.38	**<0.001**
TTHC (μmol/L, mean±SD)	191.28±61.02	238.20±59.45	1.01	1.00-1.01	**<0.001**

Table 2 Multivariate cox regression with HRs and 95% CIs of DFS according to TTHC and SR tertiles

	Tertile 1	Tertile 2	Tertile 3	*P* for trend	per SD increase
SR					
Level	2.49 (2.07-3.07)	4.22 (3.79-4.53)	6.55 (5.76-7.34)		
No. of participants	189	188	188		
No. of incidence cases	7	29	41		
Cox Regression					
Crude mode l	Reference	4.45(1.95-10.16)	6.36(2.85-14.18)	<0.001	1.64(1.40-1.93)
Adjusted model 1	Reference	4.44(1.95-10.14)	6.45(2.89-14.39)	<0.001	1.67(1.41-1.97)
Adjusted model 2	Reference	4.40(1.88-10.29)	6.65(2.85-15.50)	<0.001	1.60(1.32-1.94)
TTHC(μmol/L)					
Level	143.22(120.21-154.66)	186.53(170.81-200.62)	264.06(233.61-301.37)		
No. of participants	190	186	189		
No. of incidence cases	8	24	45		
Cox Regression					
Crude mode l	Reference	3.17(1.42-7.05)	6.25(2.95-13.26)	<0.001	1.81(1.49-2.21)
Adjusted model 1	Reference	3.18(1.43-7.08)	6.31(2.97-13.39)	<0.001	1.82(1.49-2.22)
Adjusted model 2	Reference	2.42(1.08-5.44)	4.05(1.85-8.86)	0.001	1.55 (1.25-1.92)

The levels of SR and TTHC were described as median (IQR, interquartile range)

Models: crude model, unadjusted; model 1: adjusted for age and menopausal status; model 2: additionally adjusted for Initial clinical stage, histological grade, molecular subtype, Ki-67 status, lymphovascular invasion, radiation, and chemotherapy based on Model 1

P for trend: The level of SR or TTTC was included in Cox regression with median and entered as a continuous variable

Per SD increase: Per standard deviation increase, the level of SR or TTHC was included in Cox regression after standardized as a continuous variable

respectively, compared with the reference level ($P<0.01$). For imaging features, both a higher SR (HR=1.28, 95% CI=1.17–1.38) and TTHC (HR=1.01, 95% CI=1.00–1.01) were significantly correlated with poor DFS ($P<0.01$).

Relationship between SR, TTHC, and DFS in multivariate analysis

The results of Cox regression analysis of SR and DFS are presented in Table 2. In the basic model, a higher SR was associated with poor DFS (T2 vs. T1: HR=4.45, 95% CI=1.95–10.16; T3 vs. T1: HR=6.36, 95% CI=2.85–14.18; per 1-SD increase: HR=1.64, 95% CI=1.40–1.93). The association was stronger after adjusting for baseline age and menopausal status, with the corresponding HR indicating an increased risk of DFS for both categories and per 1-SD of increase in SR ($P<0.001$ for trend). The relationship remained significant after further adjustment for potential confounding factors ($P<0.001$ for trend).

Cox regression analysis showed similar results for the relationship between TTHC and DFS (Table 2). Compared with the T1 reference group, the baseline TTHCs in the T2 and T3 groups were each associated with an increased risk of recurrence ($P<0.001$ for trend); this association persisted after adjusting for potential confounders. In the fully adjusted model, the HR per 1-SD increase was 1.55 (1.25–1.92) for DFS.

Subgroup analysis of SR and TTHC for DFS

Subgroup analysis was conducted to explore the relationship between clinicopathological and imaging features on DFS. The risk estimates of DFS in subgroup analysis are shown in Fig. 3. A significant association was observed between SR and DFS among patients who were PR-positive (2.61 vs. 2.20), HER2-negative (2.59 vs. 1.49), with lower Ki-67 expression (≦14%) (11.57 vs. 1.51), without adjuvant chemotherapy (3.49 vs. 1.76), and without Herceptin treatment (2.58 vs. 1.49). For the association between TTHC and DFS, significant interactions were observed in lymphovascular invasion, ER status, PR status, HER2 status, and Herceptin treatment ($P<0.05$).

Development and validation of a DFS prediction model

Cox regression analysis was performed to build a predictive DFS model by combining independent predictors of both clinical and imaging features. In accordance with our previous results, six classical clinical parameters (age, menopausal status, initial clinical TNM stage, histological grade, molecular subtype, lymphovascular invasion, Ki-67 status, radiation, and adjuvant chemotherapy) and imaging features (SR and TTHC) were added to the DFS model in a stepwise manner. The nomograms incorporating these predictors, separately or in combination, are shown in Fig. 4.

To compare the predictive performance of clinical, imaging, and combined clinical–imaging models, the ROC curve AUCs were analyzed (Fig. 5A). The sensitivity, specificity, accuracy, negative predictive value, and positive predictive value with the best cut-off values for each model are shown in Table 3. The TTHC+SR+C prediction model exhibited the best performance for DFS prediction (AUC=0.829), followed by the SR+C or TTHC+C models (AUC=0.824, 0.791); the model with classical clinical predictors (C) achieved an AUC of only 0.762. Decision curve analysis was performed to assess whether the TTHC+SR+C combination model was clinically beneficial and if the patients would benefit from the prediction model when the threshold probability in the clinical decision ranged from 5 to 75% (Fig. 5B). Kaplan–Meier curves stratified by the tertile of the predicted index of DFS showed good discrimination of the established combination model (Fig. 5C).

Discussion

To our knowledge, this is the first study to explore the relationship between preoperative non-invasive imaging tools (UE and DOT) and DFS among T1 BC patients with a follow-up period of nearly 10 years. The main findings were: (i) higher SRs and TTHCs correlated with a higher risk of T1 BC recurrence; (ii) the incorporated imaging–clinical model had better predictive performance than clinical prognostic indicators alone, and C+TTHC+SR showed the strongest power; and (iii) C+TTHC+SR successfully stratified the recurrence risk of patients with T1 BC, suggesting that it can provide critical support for making clinical decisions.

With the implementation of cancer-screening programs, the detection rate of T1 BC has improved. However, a certain risk of recurrence occurs despite a small tumor size [30, 31], suggesting that the ability to recurrence is an early and inherent genetic property. Observations on the outcomes of T1 BC by Houvenaeghel et al. confirmed this idea, showing a recurrence rate of 6% at 5 years and 16.2% at 10 years [2]. In our study, 77 patients (13.6%) developed recurrence over a median follow-up period of 130 months, which is similar to previous reports.

In our study, gray-scale US (BI-RADS) exhibited no significant association with DFS; nonetheless, a higher SR was identified in patients with recurrence, revealing that the SR is a more valuable prognostic indicator for predicting recurrence risk compared to BI-BAS. TTHC, as the main functional parameter of DOT, may indirectly reflect the tumor's blood supply. Our study

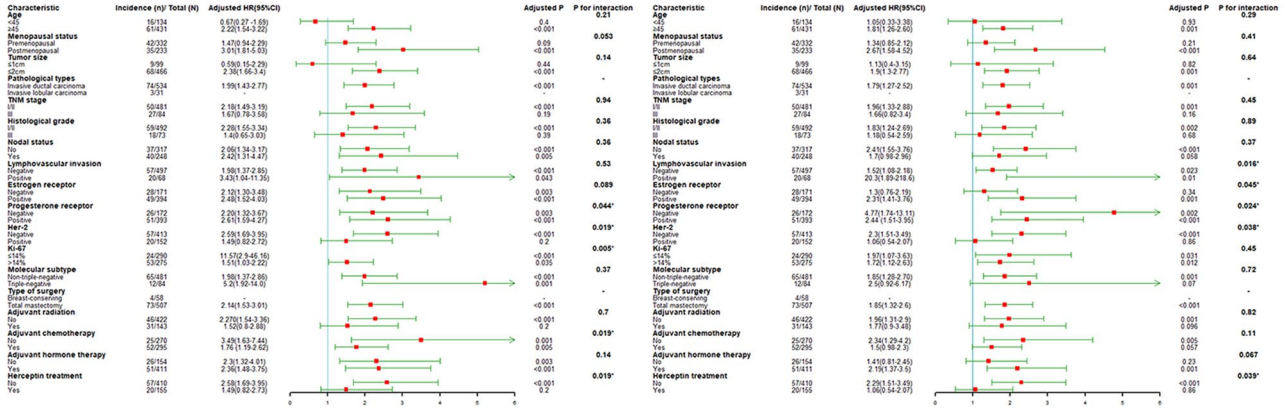

Fig. 3 Risk estimates of disease-free survival (DFS) in patient subgroups, and interaction analysis of (**A**) TTHC and (**B**) SR

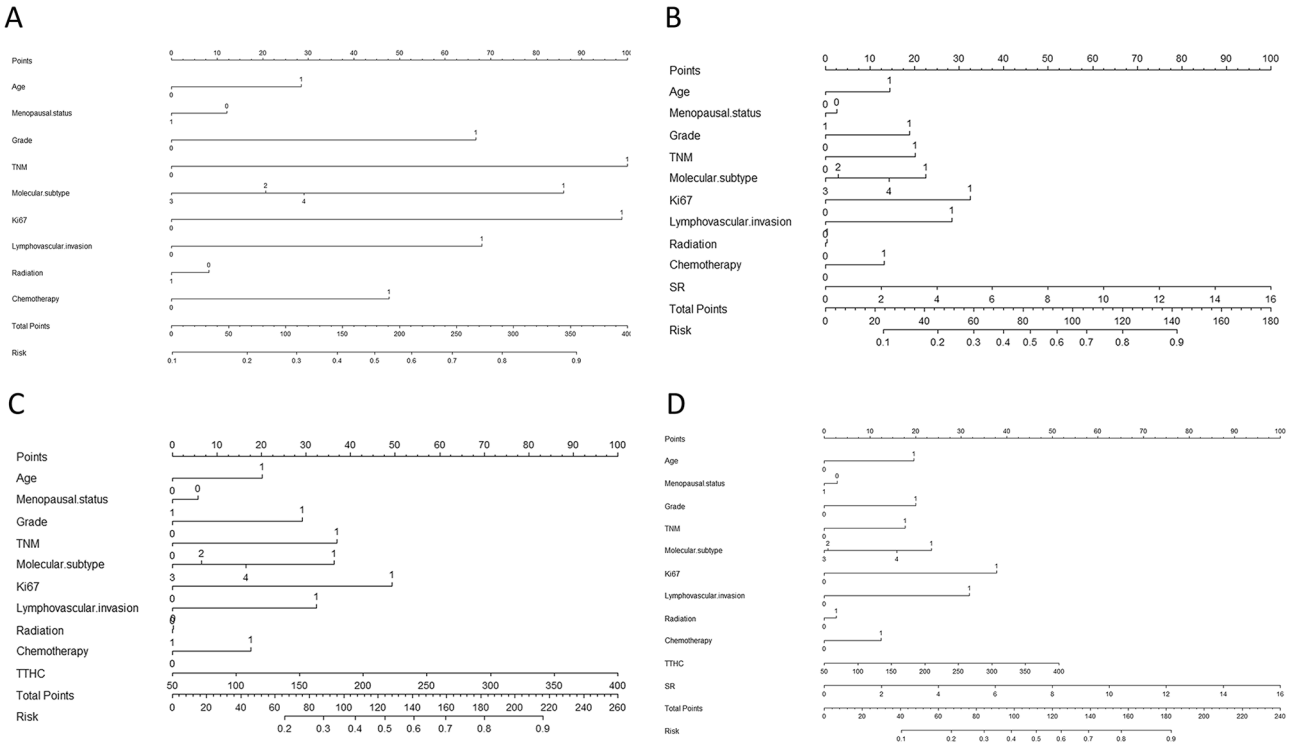

Fig. 4 Nomograms for different DFS prediction models: (**A**) classical model, (**B**) classical + SR, (**C**) classical + TTHC, and (**D**) classical + TTHC + SR. When using the nomograms, draw a vertical to a top point, and assign points for each variable; sum the points from all variables together and draw a vertical line from the top line through the total points row to obtain the probability for DFS

found that tumors with higher TTHC were present in patients with recurrence, indicating that the blood supply to tumors with poor outcomes was rich. The results can be explained as follows: to survive and proliferate in new tissue sites, tumor cells must activate more neovascularization and angiogenesis to feed themselves; tumor cells that survive in a new location are more likely to be derived from primary tumors that exhibit higher angiogenic activity [32].

This finding suggests that tumor stiffness and blood-flow features might be highly associated with DFS in T1 BC; however, current evidence on this issue is relatively scarce. To our knowledge, this study is the first comprehensive analysis to investigate the association between the TTHC, SR, and DFS in patients with T1 BC. Notably, a higher SR and TTHC were significantly associated with worse DFS outcomes, even after adjusting for clinicopathological confounding factors. The adjusted SR and TTHC still acted as independent risk factors in most subgroups. This finding supports the validity and generalizability of our findings. Furthermore, for both the SR and TTHC, intensive associations with DFS were found among patients who were HER2-negative or received non-herceptin treatment. This might inspire clinical application of the SR and TTHC; however, the mechanisms underlying these differences require further investigation.

The use of these imaging and clinical parameters for predicting DFS showed that the two non-invasive imaging tools had comparable predictive abilities. The combined imaging–clinical parameters showed better predictive ability than the clinical parameters alone. Among the models, the TTHC + SR + C model performed best. Specifically, the value of TTHC + SR + C lies more in its high negative predictive value of 96.9%. This indicates that tumors with lower stiffness and TTHC may be at a lower risk of recurrence, which is valuable information for clinical practice. In addition, the new prognostic model classified patients into high-, medium-, and low-risk groups for DFS in advance, which significantly improved its performance in predicting the risk of DFS. This strategy may help guide individualized clinical therapy and follow-up management.

To date, various noninvasive imaging modalities have been employed to predict prognosis in BC. Among these, two primary methods are based on US and optical imaging. Optical imaging utilizes near-infrared (NIR) diffused light to detect changes in blood volume within biological tissues, including DOT, diffuse optical spectroscopy, and other multimodal optical imaging technologies [33]. Some parameters derived from optical imaging show promising results in predicting the response to neoadjuvant chemotherapy in BC patients [34, 35], potentially serving as indicators for disease-free and overall survival

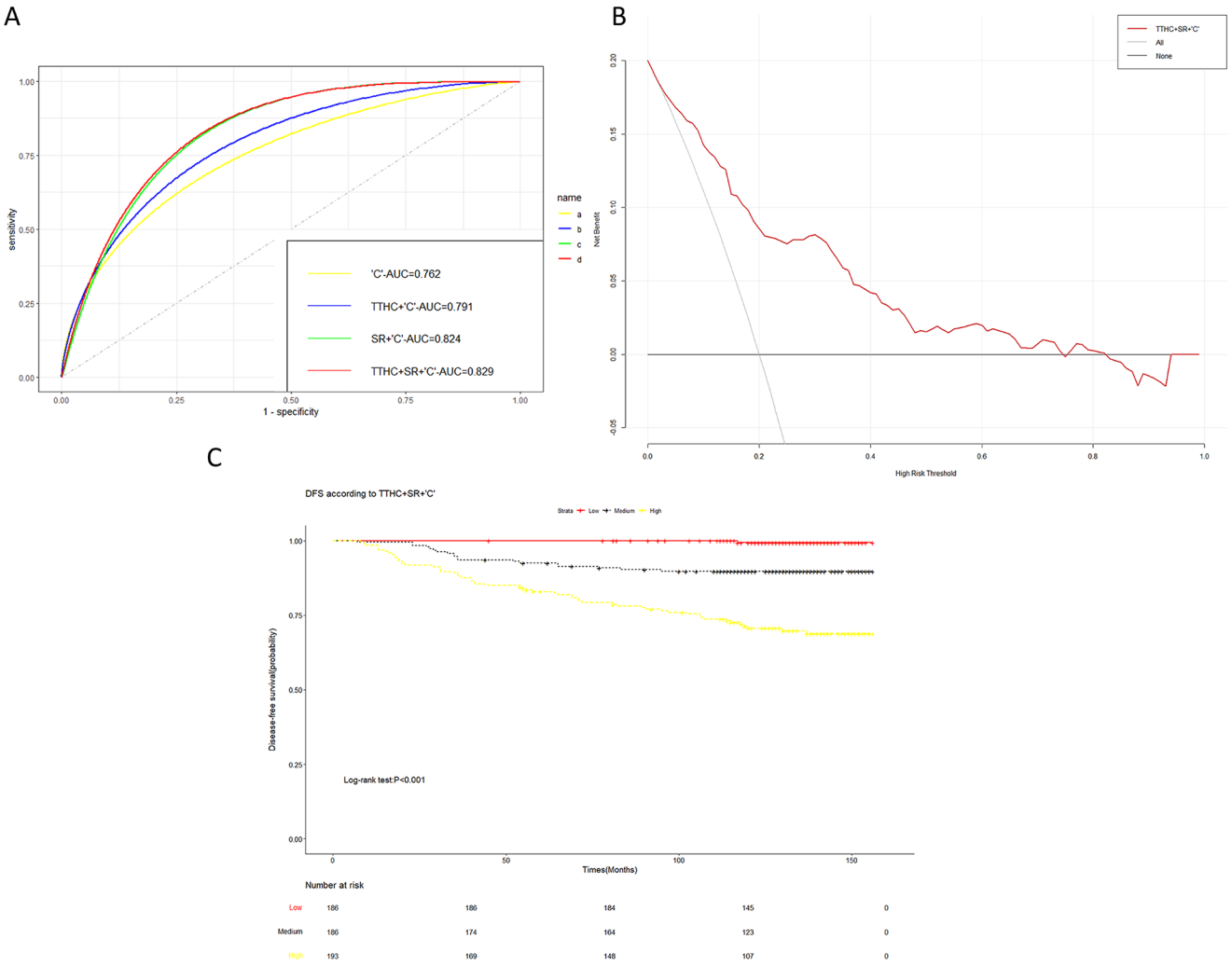

Fig. 5 Plots of performance metrics of the DFS prediction model: (**A**) receiver operating characteristic curves for comparing different models; (**B**) decision curve analysis of DFS prediction model with the best performance; (**C**) Kaplan–Meier estimate of DFS with low, medium, and high risk stratified by prediction index

Table 3 Model performance for DFS prediction with optimal cut-off points

Models	Threshold	AUC (95% CI)	Sensitivity (95% CI)	Specificity (95% CI)	Accuracy (95% CI)	NPV (95% CI)	PPV (95% CI)
C	>=0.161	0.762(0.702-0.822)	0.636(0.529-0.744)	0.814(0.779-0.848)	0.789(0.789-0.790)	0.934(0.911-0.958)	0.350(0.271-0.429)
SR+C	>=0.072	0.824(0.782-0.866)	0.974(0.938-1.00)	0.539(0.495-0.583)	0.598(0.597-0.599)	0.992(0.982-1.00)	0.250(0.201-0.299)
TTHC+C	>=0.234	0.791(0.738-0.844)	0.558(0.448-0.669)	0.883(0.855-0.912)	0.839(0.838-0.839)	0.927(0.903-0.951)	0.430(0.333-0.527)
TTHC+SR+C	>=0.092	0.829(0.786-0.872)	0.870(0.795-0.945)	0.645(0.603-0.688)	0.676(0.675-0.677)	0.969(0.950-0.988)	0.279(0.222-0.336)

AUC, the area under the ROC curve; NPV, negative predictive value; PPV, positive predictive value

outcomes. However, few studies have directly investigated the correlation between optical imaging findings and prognosis in BC.

Ultrasound-based non-invasive methodologies, such as microvascular ultrasound and shear-wave elastography (SWE), hold promise for predicting BC prognosis. Microvascular ultrasound employs advanced Doppler techniques, offering high sensitivity and spatial resolution to visualize low-flow vessels in detail [36]. This modality aids in predicting histological prognostic factors of BC, including microvessel density (MVD), histological grade, negative ER expression, and HER2 expression [37, 38], and specific genetic alterations linked to angiogenesis or tumor prognosis [39], These suggested that features of microvascular ultrasound may correlate with long-term outcomes in BC. Nevertheless, current research primarily focuses on distinguishing between benign and malignant tumors, with limited investigation into BC prognosis. SWE allows enables quantitative assessment of tissue stiffness. Several studies indicate that higher elasticity values measured by SWE correlate with poorer disease-free or cancer-specific survival in BC [5, 40, 41], However, direct evidence on this matter remains relatively scarce [40], particularly for patients with early-stage BC.

Optical coherence elastography (OCE) is a novel non-invasive imaging modality designed to investigate mechanical properties at a micro-scale. In OCE, mechanical stress is applied to tissue, and optical coherence tomography measures resultant displacements. These displacements are then used to estimate and visualize variations in elasticity, or tissue stiffness, generating an image known as an elastogram [42, 43]. In recent studies, OCE has demonstrated efficacy in BC imaging, specifically in identifying cancer progression through high stiffness values [44], distinguishing morphological subtypes of BC [45], assessing lymph node status [46], detecting cancer cells in surgical margins during breast-conserving surgery [47], and evaluating cancer response to therapy [48]. This study highlights tumor stiffness as a potential prognostic indicator for BC. Yet, to date, no studies have employed this technique to evaluate tumor absolute stiffness for predicting the recurrence of BC patients.

Based on these findings, as a further work, we will incorporate more potential non-invasive techniques in large-scale multicenter studies to assess their predictive capability, with the goal of enhancing the accuracy of BC recurrence prediction.

Additionally, the development of artificial intelligence has allowed radiomics methods to be used for identifying patients at high risk of BC recurrence [10, 49–51]. A nomogram with good performance for preoperatively predicting DFS was previously developed based on the MRI radiomics and clinical signatures [10]. However, that was a retrospective study with a short follow-up period, which could lead to biased results. Recently, US-based radiomics signatures also demonstrated a predictive ability in BC in a preliminary study [50]. In future studies, we will include more ultrasonographic parameters and explore the power of the combination of US radiomics and clinical signatures for predicting DFS in BC.

Our study had several limitations. First, there might have been a selection bias because our study was in a single center and had a limited sample size. Therefore, larger studies involving multiple centers, or population-based studies, are required to confirm our results. Second, we selected subjects with solitary, unilateral lesions; therefore, the current prediction model might be applicable only to patients with a single lesion. Models to predict DFS of multifocal or bilateral diseases should be further investigated. Third, some clinicopathological data used in our study were obtained postoperatively due to feasibility issues. The earlier data collection period in our study was between 2012 and 2014, when performing a preoperative core needle biopsy was not widely available for T1 BC in our country; therefore, the clinical prognostic factors in our prediction model were obtained from surgical specimens. Although for most clinicopathological factors, a high concordance was found between preoperative biopsy and pathological evaluation [52, 53], there might still be a degree of bias in our results. In the future, we plan to collect clinical parameters from preoperative biopsy samples to develop a more accurate prediction model. Fourth, although many clinical covariates were included in the study, we cannot rule out the possibility that unmeasured factors might contribute to the results we obtained, including BC gene markers such as the BRCA1 and BRCA2 states. More confounding factors are needed to confirm our results in a future study; Fifth, the current study included only two imaging techniques.

In the future, we plan to integrate additional non-invasive techniques into large-scale multicenter studies to compare and evaluate their predictive efficacy, aiming to find the best predictive tools for BC prognosis. Even so, our study provides comprehensive evidence of the association between the TTHC, SR, and recurrence. Furthermore, the new DFS prediction model we developed for T1 BC patients was constructed from a prospective study design with a relatively long follow-up time (10 years), which should justify further research on this topic.

In conclusion, tumors with greater stiffness and TTHC were strongly associated with recurrence in patients with T1 BC. The combined imaging–clinical parameter model might provide a non-invasive and convenient preoperative method for predicting clinical outcomes. Our study resulted in a nomogram that can assist clinicians in targeting and individualizing appropriate treatment and management for patients with early-stage BC. In the future, multicenter prospective studies with larger sample sizes are expected to provide more-powerful evidence for the clinical utility of our model.

Abbreviations

ACR	American College of Radiology
BC	Breast cancer
BI-RADS	Breast Imaging – Reporting and Data System
C	Classical clinical model
CI	Confidence interval
DFS	Disease-free survival
DOT	Diffuse optical tomography
ER	Estrogen receptor
HER2	Human epidermal growth factor receptor 2
HR	Hazard ratios
ICC	Intraclass correlation coefficient
MVD	Microvessel density
NIR	Near-infrared
OCE	Optical coherence elastography
PR	Progesterone receptor
ROI	Region of interest
SE	Strain elastography
SR	Strain ratio
SWE	Shear-wave elastography
TTHC	The total hemoglobin concentration
UE	Ultrasound elastography
US	Ultrasound

Supplementary Information

The online version contains supplementary material available at https://doi.org/10.1186/s12885-024-12844-z.

Supplementary Material 1

Acknowledgements

The authors would like to thank colleagues from the Departments of Breast surgery, Ultrasound, and Pathology for their help in data collection and technical support.

Author contributions

ZJ conceived and designed the study; SC and SH analyzed and interpreted the data; GS and KY performed the histological analysis; ZJ wrote the manuscript; SC reviewed and revised the manuscript. All authors read and approved the final manuscript.

Funding

This research received no funding.

Data availability

The data used and analyzed during the current study are available from the corresponding author on reasonable request.

Declarations

Ethics approval and consent to participate

The study was conducted according to the guidelines of the Declaration of Helsinki, and was approved by the ethics committee, Shengjing Hospital of China Medical University (No: 2020PS748K). Written informed consent was obtained from all patients.

Consent for publication

Not applicable.

Competing interests

The authors declare no competing interests.

Author details

[1]Department of Ultrasound, Shengjing Hospital of China Medical University, No.36, Sanhao Street, Heping District, Shenyang, Liaoning 110004, China
[2]Department of Clinical Epidemiology and Evidence-Based Medicine, The First Hospital of China Medical University, Shenyang, Liaoning 110001, China
[3]Department of Clinical Oncology, Shengjing Hospital of China Medical University, Shenyang, Liaoning 110004, China
[4]Department of Pathology, Shengjing Hospital of China Medical University, Shenyang, Liaoning 110004, China

Received: 25 January 2024 / Accepted: 22 August 2024
Published online: 27 August 2024

References

1. Sancho-Garnier H, Colonna M. Épidémiologie des cancers du sein [Breast cancer epidemiology]. Presse Med. 2019;48(10):1076–84.
2. Houvenaeghel G, Goncalves A, Classe JM, Garbay JR, Giard S, Charytensky H, Cohen M, Belichard C, Faure C, Uzan S, et al. Characteristics and clinical outcome of T1 breast cancer: a multicenter retrospective cohort study. Annals Oncology: Official J Eur Soc Med Oncol. 2014;25(3):623–8.
3. Hanrahan EO, Valero V, Gonzalez-Angulo AM, Hortobagyi GN. Prognosis and management of patients with node-negative invasive breast carcinoma that is 1 cm or smaller in size (stage 1; T1a,bN0M0): a review of the literature. J Clin Oncology: Official J Am Soc Clin Oncol. 2006;24(13):2113–22.
4. Banerjee S, Smith IE. Management of small HER2-positive breast cancers. Lancet Oncol. 2010;11(12):1193–9.
5. Evans A, Sim YT, Pourreyron C, Thompson A, Jordan L, Fleming D, Purdie C, Macaskill J, Vinnicombe S, Pharoah P. Pre-operative stromal stiffness measured by shear wave elastography is independently associated with breast cancer-specific survival. Breast Cancer Res Treat. 2018;171(2):383–9.
6. Fitzgibbons PL, Page DL, Weaver D, Thor AD, Allred DC, Clark GM, Ruby SG, O'Malley F, Simpson JF, Connolly JL, et al. Prognostic factors in breast cancer. College of American Pathologists Consensus Statement 1999. Arch Pathol Lab Med. 2000;124(7):966–78.
7. Sparano JA, Gray RJ, Makower DF, Albain KS, Saphner TJ, Badve SS, Wagner LI, Kaklamani VG, Keane MM, Gomez HL, et al. Clinical outcomes in early breast Cancer with a high 21-Gene recurrence score of 26 to 100 assigned to Adjuvant Chemotherapy Plus Endocrine Therapy: a secondary analysis of the TAILORx Randomized Clinical Trial. JAMA Oncol. 2020;6(3):367–74.
8. Sparano JA, Gray RJ, Ravdin PM, Makower DF, Pritchard KI, Albain KS, Hayes DF, Geyer CE Jr., Dees EC, Goetz MP, et al. Clinical and genomic risk to Guide the Use of adjuvant therapy for breast Cancer. N Engl J Med. 2019;380(25):2395–405.
9. Moller NB, Boonen DS, Feldner ES, Hao Q, Larsen M, Laenkholm AV, Borg A, Kvist A, Torngren T, Jensen UB, et al. Validation of the BOADICEA model for

predicting the likelihood of carrying pathogenic variants in eight breast and ovarian cancer susceptibility genes. Sci Rep. 2023;13(1):8536.
10. Yu Y, Tan Y, Xie C, Hu Q, Ouyang J, Chen Y, Gu Y, Li A, Lu N, He Z, et al. Development and validation of a Preoperative Magnetic Resonance Imaging Radiomics-Based Signature to Predict Axillary Lymph Node Metastasis and Disease-Free Survival in patients with early-stage breast Cancer. JAMA Netw Open. 2020;3(12):e2028086.
11. Cho HH, Kim H, Nam SY, Lee JE, Han BK, Ko EY, Choi JS, Park H, Ko ES. Measurement of Perfusion heterogeneity within Tumor habitats on Magnetic Resonance Imaging and its association with prognosis in breast Cancer patients. Cancers 2022, 14(8).
12. Yoo H, Cho KR, Song SE, Cho Y, Jung SP, Sung K. Tumor Heterogeneity of Breast Cancer Assessed with Computed Tomography Texture Analysis: Association with Disease-Free Survival and Clinicopathological Prognostic Factor. *Diagnostics (Basel)* 2023, 13(23).
13. Zhang L, Zhang X, Han P, Zhao D, Hu N, Fan W, Wang P, Zuo X, Kong H, Peng F, et al. Nomograms predicting recurrence in patients with triple negative breast cancer based on ultrasound and clinicopathological features. Br J Radiol. 2022;95(1138):20220305.
14. Lawson BT, Vinnicombe S, Whelehan P, Macaskill EJ, Sim YT, Evans A. Associations between the ultrasound features of invasive breast cancer and breast cancer specific survival. Clin Radiol. 2020;75(11):e879813–21.
15. Fu Q, Wan F, Lu Q, Shao W, Fu G, Wang Z. Correlation Analysis of Ultrasound Elastography Score with Invasive Breast Cancer and Biological Prognostic Factors. *Contrast media & molecular imaging* 2022, 2022:1174541.
16. Evans A, Whelehan P, Thomson K, McLean D, Brauer K, Purdie C, Baker L, Jordan L, Rauchhaus P, Thompson A. Invasive breast cancer: relationship between shear-wave elastographic findings and histologic prognostic factors. Radiology. 2012;263(3):673–7.
17. Jiang S, Yang Y, Fang M, Li X, Yuan X, Yuan J. Co-evolution of tumor-associated macrophages and tumor neo-vessels during cervical cancer invasion. Oncol Lett. 2016;12(4):2625–31.
18. Nakamiya N, Ueda S, Shigekawa T, Takeuchi H, Sano H, Hirokawa E, Shimada H, Suzuki H, Oda M, Osaki A, et al. Clinicopathological and prognostic impact of imaging of breast cancer angiogenesis and hypoxia using diffuse optical spectroscopy. Cancer Sci. 2014;105(7):833–9.
19. Niu S, Zhu Q, Jiang Y, Zhu J, Xiao M, You S, Zhou W, Xiao Y. Correlations among Ultrasound-guided diffuse Optical Tomography, Microvessel Density, and breast Cancer prognosis. J Ultrasound Medicine: Official J Am Inst Ultrasound Med. 2018;37(4):833–42.
20. Berg WA, Cosgrove DO, Doré CJ, Schäfer FK, Svensson WE, Hooley RJ, Ohlinger R, Mendelson EB, Balu-Maestro C, Locatelli M, et al. Shear-wave elastography improves the specificity of breast US: the BE1 multinational study of 939 masses. Radiology. 2012;262(2):435–49.
21. Cosgrove DO, Berg WA, Doré CJ, Skyba DM, Henry JP, Gay J, Cohen-Bacrie C. Shear wave elastography for breast masses is highly reproducible. Eur Radiol. 2012;22(5):1023–32.
22. Kumar S, Chatterjee M, Ghosh P, Ganguly KK, Basu M, Ghosh MK. Targeting PD-1/PD-L1 in cancer immunotherapy: an effective strategy for treatment of triple-negative breast cancer (TNBC) patients. Genes Dis. 2023;10(4):1318–50.
23. Jung NY, Park CS, Kim SH, Jung HS, Kim K, Lee JW, Shin YR, Oh SJ. Sonoelastographic strain ratio: how does the position of reference fat influence it? Japanese J Radiol. 2016;34(6):440–7.
24. Hammond ME, Hayes DF, Dowsett M, Allred DC, Hagerty KL, Badve S, Fitzgibbons PL, Francis G, Goldstein NS, Hayes M, et al. American Society of Clinical Oncology/College of American Pathologists guideline recommendations for immunohistochemical testing of estrogen and progesterone receptors in breast cancer. J Clin Oncology: Official J Am Soc Clin Oncol. 2010;28(16):2784–95.
25. Sauter G, Lee J, Bartlett JM, Slamon DJ, Press MF. Guidelines for human epidermal growth factor receptor 2 testing: biologic and methodologic considerations. J Clin Oncology: Official J Am Soc Clin Oncol. 2009;27(8):1323–33.
26. Goldhirsch A, Winer EP, Coates AS, Gelber RD, Piccart-Gebhart M, Thurlimann B, Senn HJ. Panel m: personalizing the treatment of women with early breast cancer: highlights of the St Gallen International Expert Consensus on the primary therapy of early breast Cancer 2013. Ann Oncol. 2013;24(9):2206–23.
27. Giuliano AE, Edge SB, Hortobagyi GN. Eighth Edition of the AJCC Cancer staging Manual: breast Cancer. Ann Surg Oncol. 2018;25(7):1783–5.
28. Tan PH, Ellis I, Allison K, Brogi E, Fox SB, Lakhani S, Lazar AJ, Morris EA, Sahin A, Salgado R, et al. The 2019 World Health Organization classification of tumours of the breast. Histopathology. 2020;77(2):181–5.
29. Kim SY, Han BK, Kim EK, Choi WJ, Choi Y, Kim HH, Moon WK. Breast Cancer detected at screening US: Survival Rates and Clinical-Pathologic and Imaging Factors Associated with recurrence. Radiology. 2017;284(2):354–64.
30. Ichizawa N, Fukutomi T, Iwamoto E, Akashi-Tanaka S. Long-term results of T1a, T1b and T1c invasive breast carcinomas in Japanese women: validation of the UICC T1 subgroup classification. Jpn J Clin Oncol. 2002;32(3):108–9.
31. Joensuu H, Pylkkänen L, Toikkanen S. Late mortality from pT1N0M0 breast carcinoma. Cancer. 1999;85(10):2183–9.
32. Weidner N, Semple JP, Welch WR, Folkman J. Tumor angiogenesis and metastasis–correlation in invasive breast carcinoma. N Engl J Med. 1991;324(1):1–8.
33. Vaughan CL. Novel imaging approaches to screen for breast cancer: recent advances and future prospects. Med Eng Phys. 2019;72:27–37.
34. Zhang J, Tan X, Zhang X, Kang Y, Li J, Ren W, Ma Y. Efficacy of shear-wave elastography versus dynamic optical breast imaging for predicting the pathological response to neoadjuvant chemotherapy in breast cancer. Eur J Radiol. 2020;129:109098.
35. Pavlov MV, Bavrina AP, Plekhanov VI, Golubyatnikov GY, Orlova AG, Subochev PV, Davydova DA, Turchin IV, Maslennikova AV. Changes in the tumor oxygenation but not in the tumor volume and tumor vascularization reflect early response of breast cancer to neoadjuvant chemotherapy. Breast cancer Research: BCR. 2023;25(1):12.
36. Park AY, Seo BK, Han MR. Breast Ultrasound Microvascular Imaging and Radiogenomics. Korean J Radiol. 2021;22(5):677–87.
37. Park AY, Kwon M, Woo OH, Cho KR, Park EK, Cha SH, Song SE, Lee JH, Cha J, Son GS, et al. A prospective study on the Value of Ultrasound Microflow Assessment to Distinguish Malignant from Benign solid breast masses: Association between Ultrasound parameters and histologic microvessel densities. Korean J Radiol. 2019;20(5):759–72.
38. Wan CF, Du J, Fang H, Li FH, Zhu JS, Liu Q. Enhancement patterns and parameters of breast cancers at contrast-enhanced US: correlation with prognostic factors. Radiology. 2012;262(2):450–9.
39. Han MR, Park AY, Seo BK, Bae MS, Kim JS, Son GS, Lee HY, Chang YW, Cho KR, Song SE, et al. Association between vascular ultrasound features and DNA sequencing in breast cancer: a preliminary study. Discover Oncol. 2023;14(1):52.
40. Kim JY, Kim JJ, Hwangbo L, Suh HB, Lee JW, Lee NK, Choo KS, Kim S. Tumor stiffness measured by shear-wave elastography: association with disease-free survival in women with early-stage breast cancer. Br J Radiol. 2021;94(1128):20210584.
41. Machida Y, Shimauchi A, Okuma H, Tozaki M, Isobe S, Fukuma E. Shear Wave Speed of the lesion in preoperative breast Ultrasonography: Association with Disease-free survival of patients with primary operable invasive breast Cancer. Acad Radiol. 2018;25(8):1003–9.
42. Kennedy KM, Ford C, Kennedy BF, Bush MB, Sampson DD. Analysis of mechanical contrast in optical coherence elastography. J Biomed Opt. 2013;18(12):121508.
43. Yuting L, Li C, Zhou K, Guan G, Appleton PL, Lang S, McGloin D, Huang Z, Nabi G. Microscale characterization of prostate biopsies tissues using optical coherence elastography and second harmonic generation imaging. Lab Invest. 2018;98(3):380–90.
44. Kennedy BF, McLaughlin RA, Kennedy KM, Chin L, Wijesinghe P, Curatolo A, Tien A, Ronald M, Latham B, Saunders CM, et al. Investigation of Optical Coherence Microelastography as a method to visualize cancers in human breast tissue. Cancer Res. 2015;75(16):3236–45.
45. Gubarkova EV, Kiseleva EB, Sirotkina MA, Vorontsov DA, Achkasova KA, Kuznetsov SS, Yashin KS, Matveyev AL, Sovetsky AA, Matveev LA et al. Diagnostic accuracy of cross-polarization OCT and OCT-Elastography for differentiation of breast Cancer subtypes: comparative study. Diagnostics (Basel Switzerland) 2020, 10(12).
46. Kennedy BF, McLaughlin RA, Kennedy KM, Chin L, Curatolo A, Tien A, Latham B, Saunders CM, Sampson DD. Optical coherence micro-elastography: mechanical-contrast imaging of tissue microstructure. Biomedical Opt Express. 2014;5(7):2113–24.
47. Gong P, Chin SL, Allen WM, Ballal H, Anstie JD, Chin L, Ismail HM, Zilkens R, Lakhiani DD, McCarthy M, et al. Quantitative Micro-elastography enables in vivo detection of residual Cancer in the Surgical cavity during breast-conserving surgery. Cancer Res. 2022;82(21):4093–104.
48. Plekhanov AA, Gubarkova EV, Sirotkina MA, Sovetsky AA, Vorontsov DA, Matveev LA, Kuznetsov SS, Bogomolova AY, Vorontsov AY, Matveyev AL, et al. Compression OCT-elastography combined with speckle-contrast analysis as an approach to the morphological assessment of breast cancer tissue. Biomedical Opt Express. 2023;14(6):3037–56.

49. Zhu XD, Yu JH, Ai FL, Wang Y, Lv W, Yu GL, Cao XK, Lin J. Construction and validation of a Novel Nomogram for Predicting the risk of Metastasis in a Luminal B Type Invasive Ductal Carcinoma Population. World J Oncol. 2023;14(6):476–87.
50. Xiong L, Chen H, Tang X, Chen B, Jiang X, Liu L, Feng Y, Liu L, Li L. Ultrasound-based Radiomics Analysis for Predicting Disease-Free survival of invasive breast Cancer. Front Oncol. 2021;11:621993.
51. Lee JY, Lee KS, Seo BK, Cho KR, Woo OH, Song SE, Kim EK, Lee HY, Kim JS, Cha J. Radiomic machine learning for predicting prognostic biomarkers and molecular subtypes of breast cancer using tumor heterogeneity and angiogenesis properties on MRI. Eur Radiol. 2022;32(1):650–60.
52. Shanmugalingam A, Hitos K, Hegde S, Al-Mashat A, Pathmanathan N, Edirimmane S, Hughes TM, Ngui NK. Concordance between core needle biopsy and surgical excision for breast cancer tumor grade and biomarkers. Breast Cancer Res Treat. 2022;193(1):151–9.
53. Meattini I, Bicchierai G, Saieva C, De Benedetto D, Desideri I, Becherini C, Abdulcadir D, Vanzi E, Boeri C, Gabbrielli S, et al. Impact of molecular subtypes classification concordance between preoperative core needle biopsy and surgical specimen on early breast cancer management: single-institution experience and review of published literature. Eur J Surg Oncology: J Eur Soc Surg Oncol Br Association Surg Oncol. 2017;43(4):642–8.

Publisher's note